2015 IEEE International Conference on Robotics and Automation (ICRA)
Washington State Convention Center
Seattle, Washington, May 26-30, 2015

3D M-Blocks: Self-reconfiguring Robots Capable of Locomotion via Pivoting in Three Dimensions

John W. Romanishin, Kyle Gilpin, Sebastian Claici, and Daniela Rus

Abstract— **This paper presents the mechanical design of a modular robot called the 3D M-Block, a 50 mm cubic module capable of both independent and lattice-based locomotion. The first M-Blocks described in [1] could pivot about one axis of rotation only. In contrast, the 3D M-blocks can exert on demand both forward and backward torques about three orthogonal axes, for a total of six directions. The 3D M-Blocks transform these torques into pivoting motions which allow the new 3D M-Blocks to move more freely than their predecessors. Individual modules can employ pivoting motions to independently roll across a wide variety of surfaces as well as to join and move relative to other M-Blocks as part of a larger collective structure. The 3D M-Block maintains the same form factor and magnetic bonding system as the one-dimensional M-Blocks [1], but a new fabrication process supports more efficient and precise production. The 3D M-blocks provide a robust and capable modular self-reconfigurable robotic platform able to support swarm robot applications through individual module capabilities and self-reconfiguring robot applications using connected lattices of modules.**

I. Introduction

We continue our quest to create autonomous shape-changing robots which are able to to change their configuration in order to accomplish different tasks. Many interesting robotic systems have been proposed in pursuit of this goal, as shown in the survey article [2], and more recently in [3] and [4]. This paper describes a new unit module, the 3D M-Block, which builds upon the first M-Blocks [1]. These modules were capable of movement in just one direction by pivoting along a single axis. In contrast, the new 3D M-Blocks are capable of applying pivoting torques in both forward and backward directions along any of the module's three axes.

Each 3D M-Block is a 50 mm cubic module with six identical connection faces, and no actively driven external parts. An inertial actuator located in the center of the module is able to apply a controlled torque at the center of mass of the module in both clockwise and counterclockwise directions. Furthermore, the inertial actuator can be reoriented in order to apply torque about any of the three mutually orthogonal axes that are aligned along the cubic structure. This allows the modules to move in three distinct fashions: (1) independently in various environments; (2) simultaneously as part of an assembly of modules (e.g. all units in spherical meta-modules can roll simultaneously); and (3) relative to other fixed modules in order to self-reconfigure a larger lattice structure.

J. W. Romanishin, K. Gilpin, S. Claici, and D. Rus are with the Computer Science and Artificial Intelligence Lab, MIT, Cambridge, MA, 02139 {johnrom|kwgilpin|sclaici|rus}@csail.mit.edu.

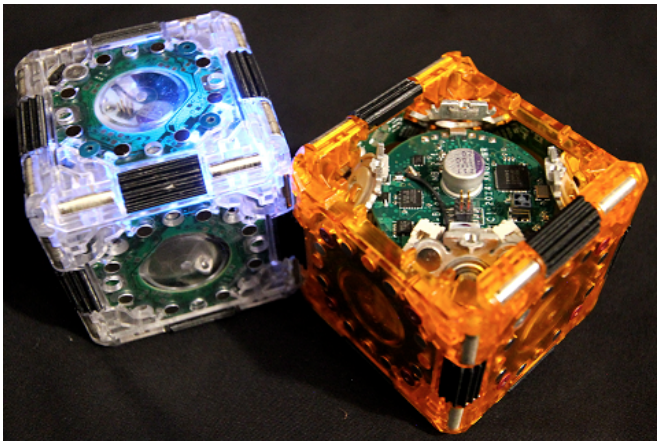

Fig. 1: The 3D M-Blocks are 50 mm self-reconfigurable modular robots which magnetically bond with their neighbors to form cubic lattices. The modules reconfigure by pivoting about their neighbors using torque generated by an internal inertial actuator. Unlike their predecessors, they can move in three dimensions.

The 3D M-Blocks move by a sequence of pivoting steps. In each step, the module pivots about one of its edges, effectively rotating by $\pi/2$ or π radians. The key mechanical design innovation for 3D M-Blocks is the internal mechanism that can be controlled to select the axis of rotation for the next movement. While the basic idea is similar to that described in [1], the inertial actuator, batteries and electronics are now able to move in relation to the module's cubic frame, allowing for three-dimensional motion. The modules have increased in functionality while striving to keep a minimum of actuated moving parts and simplifying the manufacturing process.

Recent work on the Kilobots [5] has shown the promise of large robotic swarms, which can only be realized with a combination of simple hardware and robust algorithms. For thousands of M-Blocks to operate cooperatively, the cost of manufacture and speed of assembly need to be brought down dramatically, but we are optimistic that this work is the first step in that process.

In order to analyze and quantify the pivoting capabilities of the modules, we present data from our experimental evaluations of the inertial actuator inside each module. Furthermore, to show the range of the modules' shapeshifting and traversing abilities, we present results from experiments with independent module movements as well as lattice reconfiguration movements.

This paper is organized as follows. Section II gives an overview of related work that pertains to the 3D M-Blocks

978-1-4799-6923-4/15/$31.00 ©2015 IEEE

system. Section III presents the mechanical and electrical design of the Modules. Next, Section IV presents data characterizing the hardware and the results of experiments with the system. Finally, Section V concludes with a short discussion and ideas for future work.

II. Related Work

Modular self-reconfigurable robots are often characterized by their system topology: lattice, chain, or hybrid [2]. Most of the systems currently under development including U-Bots [6], Roombots [7], and SMORES [2] utilize a hybrid architecture. The fundamental distinction between hybrid or chain modules and strict lattice systems is that hybrid or chain modules have either fewer connector faces than lattice faces, or these connector faces are located in off-lattice positions. Chain and hybrid systems are typically designed to self-reconfigure using complicated implementations which approximate simpler models, such as the sliding cube model [8] or the pivoting cube model [1].

There have been several systems which attempt to implement the sliding cube model [9], [10], [11], but these systems have been limited to two dimensions. Additionally, there are systems which are able to self-reconfigure in three dimensions [12], [13], but these systems all diverge from the simplicity offered by the sliding and pivoting cube models. We are not aware of any preexisting three dimensional hardware that is able to reconfigure in a manner that directly mimics the theoretical models. Furthermore, recent research [14] has produced a provably correct self-reconfiguration algorithm for two dimensional systems based on the sliding cube model. No such solution in three dimensions has yet been presented for the sliding cube model or for the pivoting cube model.

Many existing modular systems are also dependent on complex, mechanically active connectors which require careful alignment [6], [7], [2], [15]. In contrast, the M-Blocks use passive magnetic connectors which automatically self-align. While these magnetic connectors may not be as strong as protruding mechanical latches found in other systems, they are simple to use. Continuing advancements in advanced connector design, such as solder-based connectors [4] may provide additional options for the M-Blocks in the future.

Most existing modular systems are also limited by the inability of the modules to move independently. Like the M-Blocks, a few other system do not suffer from this drawback, for example M^3Express [15] whose wheeled modules can drive without being a part of a larger group of modules. The Cubli [16] is a recently developed robot which uses torque-producing flywheels to move and balance on its edges. It can also move independently, but unlike the M-Blocks, Cubli is not designed to operate in large ensembles and cannot climb over and around other modules.

To the best of our knowledge, the 3D M-Blocks are the only self-reconfigurable robots capable of implementing a simple movement model in three dimensions that allows for both independent and lattice-based locomotion.

III. Hardware

We have constructed four active 3D M-Blocks modules, as well as many passive modules. Although the modules share the basic shape and magnetic bonding mechanism as the previous one-dimensional system, almost every part has been completely redesigned. The significant changes include the plane changing mechanism, edge gear teeth, and simplified secondary magnet arrangement. The basic parameters of the new module, and how they compare with the previous version, are shown in Table I.

TABLE I: Comparison of 3D M-Blocks to first generation M-Blocks. † Pre-assembled ball bearings and assembled printed circuit boards are counted as single parts.

	M-Blocks	3D M-Blocks
Actuation Directions	1	6
Mass	143 g	150 g
Flywheel Moment of Inertia	5.7 E-6 kgm^2	8.4 E-6 kgm^2
Total Parts †	178	216
Actuated Moving Parts	8	10
Unique Parts	30	46
Est. Cost	$250	$130
Maximum Torque	1.6 Nm	2.6 Nm

The goal of redesigning the M-Blocks was to extend their functionally to three dimensions while maintaining robustness and keeping the components as simple and mass-producible as possible. In order to extend the original M-Blocks concept to three planes, we first considered three separate, mutually orthogonal inertial actuators, similar to the design for Cubli [16]. However it proved difficult to fit three separate sets of flywheels, motors, and brakes inside the 50 mm modules while maintaining a torque density sufficient to perform lattice reconfiguration. Despite the added complexity of having to change planes, the advantage in power of a larger single flywheel proved to be the better solution.

The redesign has focused on replacing complex actuators with simple ones while also attempting to utilize under-actuation where possible. For example, the flywheel brake in the 3D M-Blocks is built from a coil, two magnets, and a simple linkage. In contrast, the original M-Blocks employed a hobby-style servo motor which was large and prone to failure. Additionally, the orientation of the flywheel with respect to the module's frame is now controlled by the primary inertial actuator and a locking mechanism instead of an additional motor.

While the 3D M-Blocks have more parts and more mass than their predecessors, they are capable of producing a higher maximum torque, controlled by more robust and capable electronics, and require less expensive machining. The modules have proven to be robust, undergoing hundreds of reconfiguration movements without degradation, and surviving many falls of up to one meter in height. The remainder of this section will describe the mechanical structure of the modules, the design of the inertial actuator, the operation of the plane changing mechanism, and the details of the electronics which control the modules.

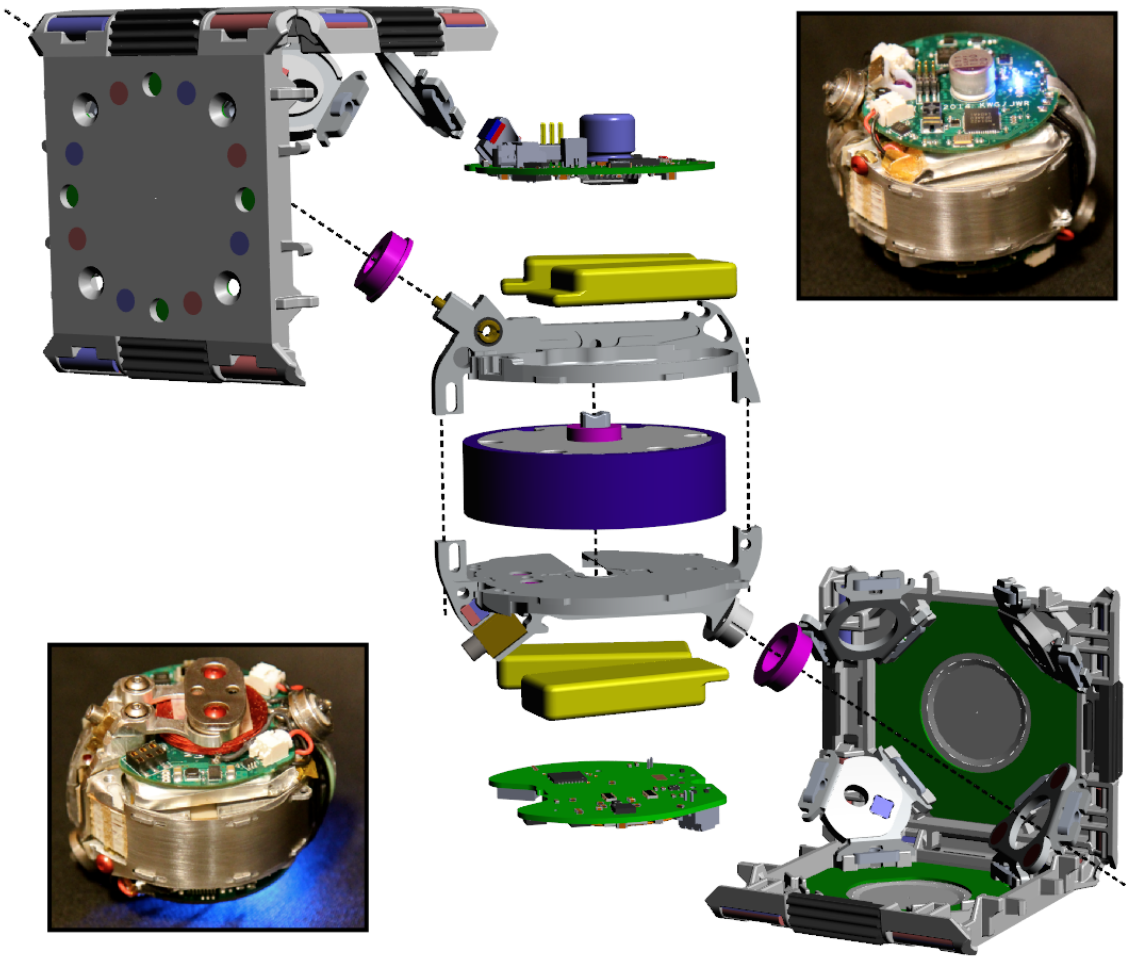

Fig. 2: Each 3D M-Block is built around a six-piece injection molded frame *gray* which supports the central assembly *lighter gray, split in half* along the frame's longest diagonal axis on two ball bearings *pink*. The molded frame holds eight magnets colored red and blue to represent their magnetic polarities. The central assembly holds batteries *yellow* and circuit boards *green* as well as the flywheel *purple*. The flywheel represents the inertial actuator. For clarity, the brake assembly is not shown in the exploded-view, it can be seen in the bottom-left inset picture. The top-right inset picture shows the main PCB.

A. Overall Module Design

The 3D M-Blocks consist of four primary mechanical assemblies: a frame (1) which holds the central assembly (2) which in turn supports the flywheel (3) and the braking mechanism (4). In addition, the central assembly holds the four batteries which power the module and two of the printed circuit boards (PCBs) which control it. The exploded view in Figure 2 shows the frame, central actuator, flywheel, batteries, and control PCBs. The two insets in Figure 2 show actual photos of the finalized central assembly with all components including the braking system. The braking mechanism is omitted from the exploded view because it is shown in better detail in Figure 3.

At the core of the central assembly is a brushless motor and flywheel which, together with the braking mechanism, generate the torques required for all module movements and central assembly plane changes. The entire central assembly is supported by two ball bearings on a diagonal rotational axis which extends through two opposite corners of the cubic frame. As the central actuator rotates about this diagonal axis, the flywheel aligns with each of the module's coordinate axes.

B. Frame

The 50 mm cubic frame is built from six identical injection-molded panels which snap together. Each panel contains two functional edges which contain two diametrically magnetized cylindrical magnets. Furthermore, each panel holds eight smaller alignment magnets in the faces. The details of this magnetic interface configuration are described in [1]. This magnetic interface allows neighboring modules to pivot about the cylindrical magnets in their common edges, and to form face to face bonds.

In the 3D M-Blocks, we have added 15 mm wide sections of gear teeth along each module's edges (shown in black in Figure 2). These gear teeth prevent slippage as two modules pivot relative to one another. Because the shape of the gear teeth does not protrude past the extents of the frame, it does not hinder the ability of modules to pivot next to adjacent

stationary modules.

Finally, each frame panel holds a face PCB which is used to interface with the surrounding environment.

Each of the eight corners of the frame contains an aluminum corner brace. These braces are cut from sheet metal and die-formed so that they can be rigidly attached to the three adjacent panels. In addition to adding strength to the frame, two of these corner braces provide rigid mounting points for ball bearings which connect the central assembly to the frame. Three additional corner braces contain specialized mating holes and magnets which are a part of the plane changing mechanism detailed in Section III-D.

C. Inertial Actuator Design

The inertial actuator consists of a flywheel and a self-tightening band brake. All of the relevant components which form the actuator are illustrated in Figure 3.

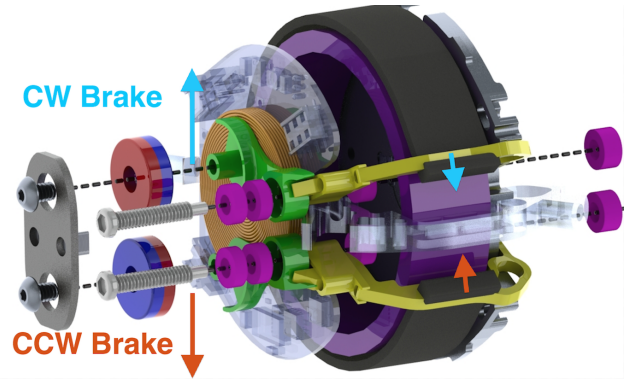

Fig. 3: The inertial actuator operates by quickly decelerating a spinning flywheel *purple* with a neoprene belt *dark gray* that wraps around the flywheel and which is anchored in two arms *yellow*. The belt is tightened by a linkage *green*, which is supported by ball bearings *pink*, and which acts as a lever to amplify the force felt at the belt (*blue* and *red* arrows indicated relative motions for both CW and CCW braking actions). To activate the brake, the coil *orange* briefly generates either a positive or negative magnetic field which exerts a corresponding force on the two magnets *red/blue* which drives the linkage.

The flywheel assembly consists of a thin brass ring with an outer diameter of 38.0 mm, inner diameter of 34.0 mm and a thickness of 10.5 mm into which the motor's rotor is press-fit. This flywheel-rotor assembly is then connected by two bearings, one on either side of the stator, to the surrounding frame such that the flywheel is completely supported and not cantilevered. This design allows for the motor and flywheel to have a thin profile while maintaining a stiff attachment to the frame. The downside to this approach is that the three wires which power the stator must fit through the center of the bearings, thereby complicating the assembly process.

Once the flywheel is spinning, the 3D M-Blocks use a direct drive electromagnetic coil actuator as shown in Figure 3 to activate the brake. We chose this approach for its fast linear response (10 ms), adequate force (3 N), bidirectionality, low cost, robustness, and size.

To exert a torque on the 3D M-Block, the motor first accelerates the flywheel to a set speed. With the motor coasting, the module energizes the pancake-shaped coil with 280 turns of #30 AWG wire to create a magnetic field. This magnetic field exerts forces on the two ring magnets and associated keeper, with one of the magnets attracted towards the center of the coil and the other repelled. The resulting force is transferred and magnified by a ratio of two to one by the four-bar linkage to the belt-holder arms. The two belt-holder arms are each attached in a one-way lever configuration to their respective elements in the four-bar linkage, thus allowing for bi-directional motion, despite the physical constraints of the belt-arms. With one of the belt holder arms pulling on its end of the belt, the mechanism tightens the belt around the flywheel. The other end of the belt is immobilized by a mechanical hard stop.

The current flowing through the coil is always polarized such that the end of the belt which is pulled causes the belt to constrict in the same direction that the motor is spinning. As the belt comes into contact with the flywheel, the friction between the two surfaces causes the belt to self-tighten and completely arrest the flywheel in a matter of milliseconds.

This system represents a complete redesign from the previous iteration. The redesign was necessary in order to fit the inertial actuator within the spherical constraint imposed on the design. As part of the redesign, the flywheel has been made larger, thicker, and, as a result, has a higher moment of inertia which allows for larger peak torques to be applied to the module. The flexible neoprene belt used for braking is now 25% wider and 30% longer, which increases its surface area, resulting in increased stopping power with less belt wear.

D. Plane Changing Mechanism

The central assembly in each 3D M-Block can be thought of as a sphere rotating inside of a cube (the frame). In order to fully constrain the two assemblies together three points of contact are required. Two of these points are formed by ball bearings attaching the central assembly to the frame through an axis aligned between two opposing corners of the frame (along the longest diagonal). This diagonal axis is offset $35\pi/180$ radians from that of the flywheel's axis of rotation. This diagonal axis extends through two opposite corners of the cubic frame. As the central actuator rotates every $2\pi/3$ radians about this diagonal axis, the flywheel aligns with a different set of the module's faces. That is, if the flywheel is initially aligned with the module's x-axis, rotating the central actuator by $2\pi/3$ radians, in one direction or another, will bring the central actuator into alignment with the module's y- or z-axis.

To lock the central assembly into place, a third connection point is necessary. It is formed by a retractable pin which protrudes from the central actuator. When extended, the pin mates with one of three matching holes in the frame's corner braces (see Figure 4).

In order to switch planes, the 3D M-Block first spins-up the motor. Once the flywheel has reached a constant speed, the pin is retracted, which allows the central assembly to spin freely on its diagonal rotation axis. A torque is then generated

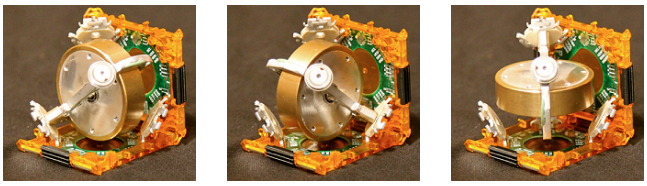

(a) X-axis (b) Y-axis (c) Z-axis

Fig. 4: The 3D M-Block changes the alignment of its flywheel by rotating the central assembly along a diagonal axis between two opposite corners of the frame (pointing out of the page). For every $2\pi/3$ radians of rotation along this axis, the flywheel comes into alignment with a new axis of the frame.

by electronically braking the motor. The component of this torque aligned with the diagonal axis, causes the central assembly to rotate and align with a new plane. Magnets, one embedded in the central assembly, and one next to each of the pin alignment holes in the frame, provide mechanical detents to assist with fine alignment between the central assembly and the frame. Once the pin is aligned with one of the mating holes, it is then extended to lock the central assembly into place.

During experiments with the 3D M-Blocks, we found that the central actuator sometimes stopped rotating about the diagonal axis at points which left the pin misaligned with the mating holes in the corners of the frame. To combat this, we added additional repulsive magnets near one of the bearings which complement the attractive force already provided by the magnets near the pin mating holes. While this change greatly reduced the frequency with which the central actuator ends up misaligned with the frame, it has also made it difficult for a module to change the plane of its central assembly if the module is not magnetically attached to a larger lattice. Without additional mass to help immobilize the module, attempting to change the plane of the central actuator results in the entire module pivoting about one of its edges. We plan to refine the magnet arrangement in order to eliminate this problem in the future.

The retractable pin is controlled by a shape memory alloy (SMA) wire which contracts when heated. The particular SMA wire is a 100 mm long, 0.25 mm diameter FLEXINOL, which is contained within a heat-resistant, insulating PEEK plastic tube. This tube insulates the wire from the metal structure of the central assembly, and it also allows the wire to bend a complete π radians in order to fit the necessary length of wire within a constrained area. One end of the SMA wire is electrically connected to a constant current driver on the main circuit board. The other end of the wire is crimped into the retractable pin, which touches the central aluminum frame, and provides an electrical ground. A strong (425 N/m) spring provides the necessary restoring force to extend the pin when the SMA is not being heated. As such, the SMA only consumes current when the pin is being held in the retracted position.

E. Electronics

The electronics, which control each 3D M-Block, are divided across eight different PCBs. The core functionality comes from a main PCB attached to one side of the central actuator. The main PCB holds a Nordic nRF51422 (nRF) microprocessor with an on-chip 2.4 GHz radio. The radio is capable of supporting both low-energy Bluetooth Smart (which we use for centralized control) and the ANT protocol (which we plan to use for module-to-module communication). The nRF is connected via a two-wire bus to a 6-axis inertial measurement unit (IMU), the MPU-6050, produced by Invensense. The IMU allows the nRF to determine the central actuator's orientation as it rotates.

The central brushless motor control is managed by a dedicated Allegro MicroSystems A4960 which frees the main processor for higher-level tasks. While the A4960 handles the low-level motor control, closed-loop speed regulation requires supervision from the nRF. The A4960 can apply an electronic braking torque to the motor in order to decelerate it more slowly than the mechanical brake.

The main PCB also includes circuitry to control the shape memory alloy (SMA) wire, which retracts the pin. The pin locks the central actuator into alignment with each of the 3D M-Block's coordinate planes. The circuitry is based on a high-current LED driver and a low-side current sense amplifier. It is capable of driving a maximum of 1.5 A through the SMA wire, but due to the relatively slow thermal response of the SMA, we modulate the current on and off to achieve sufficient force without overheating the SMA wire. When retracting the pin, we apply an average of 1.2 A for 2 s, but once retracted, we have found that we only need to apply an average of 700 mA to hold the pin stationary.

Finally, the main PCB includes charging and balancing circuitry for the four 125 mAh lithium-polymer batteries which power each 3D M-Block. The batteries are connected in series in order to supply sufficient voltage to drive the motor at speeds over 20,000 RPM. Charging is enabled by connecting the M-Block to a 5 V, 500 mA source (e.g. a USB port). An on-board, current-limited boost converter controls the voltage and current delivered to the batteries. If the nRF detects that one battery's voltage is exceeding that of the others, it switches in an additional resistive load across that battery thereby reducing its charge rate and keeping all batteries balanced.

A battery protection IC independently monitors each battery's voltage and current drain and disconnects all batteries if it detects a fault condition. The main PCB also includes additional reverse-voltage, over-current, over-temperature, and electrostatic discharge protection devices in recognition of the fact that the M-Blocks must remain robust when being deployed outside of the laboratory environment.

To complement the main PCB, there is a daughter PCB attached to the opposite side of the central actuator. The two PCBs communicate over the aforementioned two-wire bus with the nRF acting as the bus master. In addition to providing the connection point for two of the four batteries,

the daughter PCB holds the circuitry which drives current through the mechanical braking coil. The braking circuitry is controlled by an STMicroelectronics STM32F051 microprocessor which is a slave on the two-wire bus. The braking circuitry is based on an op-amp which linearizes a current-controlling PMOS device in order to provide continuous current control from 0 to 4 A.

The main and daughter PCBs are complemented by six face PCBs, which are embedded into each face of the frame. At the moment, the face PCBs provide convenient electrical contacts through which to charge the batteries. In the near future, Atmel ATtiny1634 processors on each of the face PCBs will enable infrared communication between neighboring M-Blocks. There is also a footprint for a second IMU on the face PCBs so that the central actuator will be able to determine its position relative to that of the surrounding frame. Like the processor on the daughter PCB, the Atmel processors will be slaves on the same two-wire communication bus.

The face PCBs are electrically connected to the central assembly by custom slip rings formed by the bearings that support the central assembly. One bearing is in direct electrical contact with the central assembly and provides a ground connection, while the other is isolated and carries one of the bus lines to the face PCBs. We employ a brass pin, which passes through the center of the each bearing to carry 3.3 V to the face PCBs. The pin contacts a leaf spring soldered to one of the face PCBs. Experiments have shown that the bearings present several Ohms of resistance. However, the face PCBs do not require high currents, so this is not problematic. When power is flowing into the central assembly during the charging process, the voltage drop across the bearings can be compensated for by an increase of the external charging voltage.

IV. Experiments

This section presents the results of both system-level experiments and hardware characterization for the 3D M-Block system. We performed nine sets of lattice reconfiguration experiments, and have recorded the success rate of each movement in Table II. Additionally, we experimentally measured the torque profile of the inertial actuator under several different input parameters. The magnetic bonding system was previously characterized in [1], and has since not undergone significant changes, therefore we do not repeat those measurements here. Furthermore, we discuss several less formal experiments involving 3D M-Blocks moving independently and as assemblies.

A. Lattice Reconfiguration Experiments

We performed a series of nine representative lattice reconfiguration experiments with a single module, as shown in Table II. Each reconfiguration movement was tested at least twenty times, and the overall success rate for all of the motions combined is over 88%. The success rate has increased for every movement as compared to the corresponding experiments in [1], except for the horizontal traverse, and the horizontal concave motions, see Table II. The success rates of these motions was lower, which we attribute to the higher module weight, and interference with the edge teeth while performing rotations of π radians. Additionally, the modules are now able to perform the stair step motion, which requires more torque than the previous M-Blocks were able to provide. However, since the pivoting motion exerts significant forces and torques on the entire lattice structure, some of these motions will not perform as tested under differing lattice configurations. For example, if the lattice contains only a few modules, it may be too weak to maintain its structural integrity during some transitions, or it may not be massive enough to serve as an immobile substrate on which individual modules move. We believe that generic 3D lattice reconfiguration will be possible in a system containing many M-Blocks, as long as the motion planner is capable of recovering from occasional movement failures.

B. Characterizing the Inertial Actuator

In order to reconfigure the 3D M-Block about a lattice structure, a torque is required which is powerful enough to overcome the substantial magnetic bonds attaching the module to its neighbors, but not so powerful that the module disconnects from the structure completely. The inertial actuator can generate torque through two methods: accelerating or decelerating the flywheel electronically, or by application of the mechanical brake to the rotating flywheel. As shown in Figure 5, the acceleration and the electronic braking of the flywheel generate for a period up to 1 s maximum torques on the order of 0.03 Nm, and 0.04 Nm, respectively. While these torques are not sufficient to perform any lattice reconfiguration movements, they allow the module to locomote independently, and to change planes. The application of the mechanical brake, in contrast, generates torques over a much shorter duration (10–30 ms) but which approach a maximum of 2.6 Nm. This magnitude of torque allows the modules to perform all but the most difficult lattice moves. For example, an upward stair-step while connected by four faces (below, front, left, and right) is not currently possible.

The mechanical brake generates torque through a self-tightening band brake as described in Section III-C. The torques generated by the mechanical brake display inherent variability due to variable tolerances of the components amplified bt the non-linear nature of many of the interactions. While we do not have complete control over the resultant torque, we do have control over three variables which govern the braking event: the flywheel rotational speed (up to 20000 RPM); the current supplied to the brake (up to 4 A); and brake actuation time (up to 250 ms). We have performed an initial characterization of the torque generated with the mechanical brake by directly measuring torque for several different input combinations using a load-cell based Futek TFF500 torque sensor sampling at 10 kHz (see Figure 6). Although we have not explored the complete mapping between all of the inputs and the resulting torque, we have determined sufficient input parameters for lattice movements through trial and error. Since the values for

TABLE II: Experimental results for controlled tests of various motion primitives are shown. A video of some of these experiments can be found under the link in the supplementary materials section.

	Traverse	Horizontal Traverse	Vertical Traverse	Horizontal Convex	Vertical Convex	Horizontal Concave	Vertical Concave	Corner Climb	Stair Step
Illustration	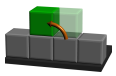				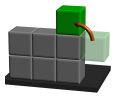			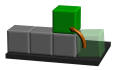	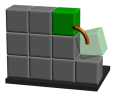
Attempted	41	20	20	20	20	20	20	20	20
Success	100%	70%	80%	95%	100%	55%	90%	100%	95%

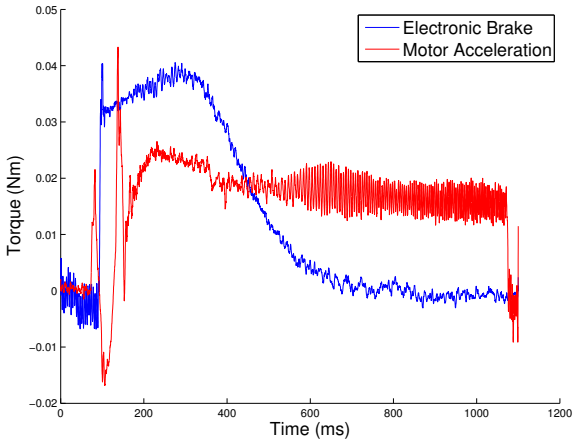

Fig. 5: This graph shows the torques generated by the inertial actuator through acceleration and electronic braking, without any use of the mechanical brake. These torques are sufficient to move a single module across the ground in an unstructured environment. Additionally, these torques are sufficient to cause the central assembly to change planes when the locking pin is retracted.

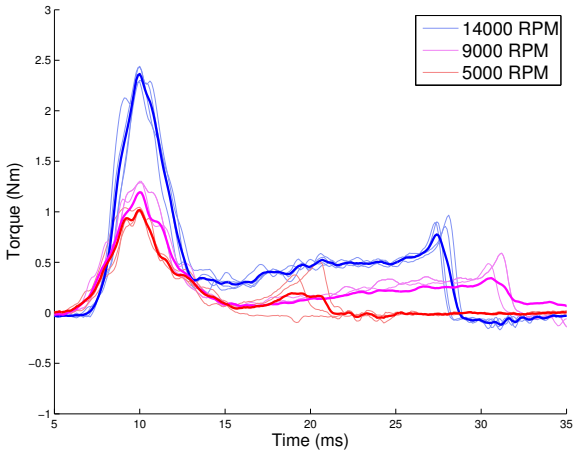

Fig. 6: This graph shows the torque generated by the inertial actuator for different input parameters measured at a rate of 10 kHz. The bold lines represent the mean values of the torque. The 14000 RPM experiment actuated the brake with 4000 mA current for 250 ms, while the 9000 RPM, and 5000 RPM experiments actuated the brake for 2000 mA for 250 ms.

lattice reconfigurations were experimentally determined, the repeatability of an output given the same input is important for consistent system performance. A qualitative sense of the repeatability of the actuator can be seen in Figure 6. While Figure 6 only shows data from a single cube, there is additional variability between the actuators of different modules. We hope to eliminate this variability through more consistent manufacturing and calibration of each module.

C. Plane Changing

The plane changing process is under-actuated, (see Section III-D), and we do not have precise control over its performance. In order to change planes, we apply a torque using the electronic brake while the locking pin is retracted, wait until the internal assembly stabilizes into a position, and then use the IMU in order to verify whether the orientation is as desired. In the case that it does not achieve the correct orientation, the module continues trying to change planes until the correct orientation is achieved. We performed ten experiments where we cycled through desired orientations. The module was able to correctly align its orientation in all ten attempts, with an average time to do so of 21.7 s, with a standard deviation of 17 s. Currently the ability to change planes works optimally while the module is attached to a lattice structure, although it is still possible while the module is independent.

D. Additional Experiments

In addition to the individual module lattice reconfiguration moves presented in Table II, we have tested several movement capabilities in a less formal manner. The 3D M-Blocks are able to move independently using several motion primitives. While moving independently, 3D M-Block modules are able to move forwards or backwards along the actuator plane in steps ranging from a single controlled roll about an edge (50 mm), to a more stochastic single movement of up to 1.5 m at full actuator power. Additionally, when the inertial actuator is oriented parallel to the ground plane and the motor is quickly accelerated for 1 s, the modules perform a random walk by rolling about their corners, and travel a distance of approximately 0.5 m along a random heading while coming to rest in a random orientation. Using these movements, the 3D M-Blocks should be able to disperse, thoroughly explore an environment, and then re-aggregate into a single structure.

Multiple 3D M-Blocks are able to perform lattice reconfiguration movements in parallel as a meta-module. We have performed a proof of concept experiment with two modules

executing a coordinated traverse. However, in order to reliably perform coordinated movements we need to further develop the software in order to ensure consistent synchronization between modules. Examples of these motions, as well as samples of the lattice reconfiguration experiments, can be found in the video linked in supplementary materials.

V. Discussion

We have introduced the 3D M-Blocks: three-dimensionally symmetric, self-contained, wireless-enabled, 50 mm cubic self-reconfigurable robots. The 3D M-Blocks extends and improve upon our previous work described in [1]. Both individual 3D M-Block modules and groups of modules are able to reconfigure on a cubic lattice of similar modules in three dimensions. To do this, the modules employ the simple pivoting cube reconfiguration model. Additionally, individual modules are able to traverse in unstructured environments using a variety of motion primitives, including jumping, controlled rolling, and random rolling at speeds approaching 1 m/s. Finally, multi-module assemblies can move in unstructured environments using coordinated actuation.

While the 3D M-Blocks system shows promise to fill a current void in the set of lattice-based self-reconfigurable robotics hardware, there remain difficulties and limitations. One fundamental limitation is the stochastic nature of many of the motion primitives on which the modules depend. While some motions achieve 100% accuracy, others are closer to 50% or do not work at all. We hypothesize that this lack of accuracy is due to the effects of relatively small manufacturing tolerances amplified by the non-linear physical interactions involved in reconfiguration. However, we are optimistic that these shortcomings can be mitigated by using a high-level planner which employs statistical models of the motion success rates in order to optimize the reconfiguration success rate, in addition to more consistent manufacturing processes.

Additionally, because 3D M-Blocks rely on permanent magnet connections and have no ability to permanently bond to their neighbors, the lattice structures which they form may be mechanically limited in two ways. First, given the finite nature of the inter-module bond strength, there are limits to which configurations are statically stable. More interestingly, the inter-module bonds in a structure must be able to withstand the impulsive forces experienced during reconfiguration, which may often exceed the static bonding forces. Consequently, a planner which accounts for the impulses experienced during reconfiguration may prove necessary.

We are interested in adding additional sensor and communication capabilities to the modules. We have imminent plans to develop the face PCBs to enable light-based environmental sensing, ensemble localization, and neighbor-to-neighbor communication. We also plan to build an extended set of modules in order to implement a variety of high-level planning algorithms on real hardware. Due to their natural tendency to self-align, combined with their robust nature, we expect that the modules will work well as the number of modules in the system scales upward. We are hopeful that the contributions we have presented here, combined with some additional refinements, will result in a lattice-based modular robotic system which is robust, simple to use, and highly capable.

Acknowledgments

This work is supported by the NSF through grants 1240383 and 1138967. The authors would like to thank Bianca Homberg and Thomas Bertossi.

Supplementary Material

`http://youtu.be/y27gUFO6mTA`

References

[1] J. W. Romanishin, K. Gilpin, and D. Rus, "M-blocks: Momentum-driven, magnetic modular robots," in *Intelligent Robots and Systems (IROS), 2013 IEEE/RSJ International Conference on*. IEEE, 2013, pp. 4288–4295.

[2] M. Yim, W. Shen, B. Salemi, D. Rus, M. Moll, H. Lipson, E. Klavins, and G. S. Chirikjian, "Modular Self-Reconfigurable Robot Systems: Challenges and Opportunities for the Future," *Robotics and Automation Magazine*, vol. 14, no. 1, pp. 43–52, 2007.

[3] M. Yim, P. White, M. Park, and J. Sastra, "Modular self-reconfigurable robots," in *Encyclopedia of complexity and systems science*. Springer, 2009, pp. 5618–5631.

[4] J. Neubert, A. Rost, and H. Lipson, "Self-soldering connectors for modular robots," *Transaction of Robotics*, vol. PP, no. 99, pp. 1–14, 2014.

[5] M. Rubenstein, A. Cornejo, and R. Nagpal, "Programmable self-assembly in a thousand-robot swarm," *Science*, vol. 345, no. 6198, pp. 795–799, 2014.

[6] Y. Zhu, J. Zhao, X. Cui, X. Wang, S. Tang, X. Zhang, and J. Yin, "Design and implementation of ubot: A modular self-reconfigurable robot," in *Mechatronics and Automation (ICMA), 2013 IEEE International Conference on*. IEEE, 2013, pp. 1217–1222.

[7] M. Vespignani, E. Senft, S. Bonardi, R. Moeckel, and A. J. Ijspeert, "An experimental study on the role of compliant elements on the locomotion of the self-reconfigurable modular robots roombots," in *Intelligent Robots and Systems (IROS), 2013 IEEE/RSJ International Conference on*. Ieee, 2013, pp. 4308–4313.

[8] R. Fitch, Z. Butler, and D. Rus, "Reconfiguration planning for heterogenous self-reconfiguring robots," in *Intelligent Robots and Systems*, 2003, pp. 2460–2467.

[9] K. Hosokawa, T. Tsujimori, T. Fujii, H. Kaetsu, H. Asama, Y. Kuroda, and I. Endo, "Self-organizing collective robots with morphogenesis in a vertical plane," in *International Conference on Robotics and Automation*, 1998, pp. 2858–2683.

[10] Y. Suzuki, N. Inou, H. Kimura, and M. Koseki, "Reconfigurable group robots adaptively transforming a mechanical structure," in *Intelligent Robots and Systems*, 2008, pp. 877–882.

[11] B. K. An, "Em-cube: Cube-shaped, self-reconfigurable robots sliding on structure surfaces," in *IEEE International Conference on Robotics and Automation (ICRA)*, May 2008, pp. 3149–3155.

[12] H. Kurokawa, K. Tomita, A. Kamimura, S. Kokaji, T. Hasuo, and S. Murata, "Distributed self-reconfiguration of m-tran iii modular robotic systems," *International Journal of Robotics Research*, vol. 27, no. 3-4, pp. 373–386, March-April 2008.

[13] H. Kurokawa, S. Murata, E. Yoshida, K. Tomita, and S. Kokaji, "A 3-d self-reconfigurable structure and experiments," in *Intelligent Robots and Systems*, October 1998, pp. 860–865.

[14] F. Hurtado, E. Molina, S. Ramaswami, and V. Sacristan, "Distributed universal reconfiguration of 2d lattice-based modular robots," in *29th European Workshop on Computational Geometry*, March 2013, pp. 139–142.

[15] K. C. Wolfe, M. S. Moses, M. D. Kutzer, and G. S. Chirikjian, "m^3express: A low-cost independently-mobile reconfigurable modular robot," in *International Conference on Robotics and Automation*, May 2012, pp. 2704–2710.

[16] M. Gajamohan, M. Merz, I. Thommen, and R. D"Andrea, "The cubli: A cube that can jump up and balance," in *Intelligent Robots and Systems*, October, pp. 3722–3727.